

Integration Aspects of Lift Augmentation Systems on the Aerodynamics of a High-Lift Configuration

By **D. Keller** AND **R. Rudnik**[†]

Institut für Aerodynamik und Strömungstechnik, DLR Braunschweig
Lilienthalplatz 7, 38108, Braunschweig

The scope of this report is to illustrate the installation effects of circulation control and turboprop engines on the stability characteristics of the reference aircraft's landing configuration in lateral motion and in failure cases. Therefore, RANS simulations of the full configuration at different side slip angles and with asymmetric boundary conditions of the circulation control system and the propellers were performed. It is shown that the lateral stability of the investigated configuration is influenced by both aspects. While thrust generally leads to a reduced stability, activated circulation control tends to amplify the aircraft's behavior. As a result, the configuration is unstable under certain conditions. The simulation of the *one engine inoperative* case demonstrated yawing moments up to twice as high as the actual yawing moments due to the asymmetric thrust. Furthermore, the report highlights the impact of the design update on the aerodynamic behavior in longitudinal motion, where an increase of maximum angle of attack and maximum lift could be achieved. Additional configuration enhancements were realized due to the design and integration of a nacelle strake.

1. Introduction

In the frame of the Collaborative Research Center 880 (CRC 880), several technologies are investigated to support a short take-off and landing transport aircraft design. Therefore, the multidisciplinary analysis of the full aircraft configuration plays a vital role, since the feasibility of the single technologies has to be assessed not only separately, but fully integrated as well. An important aspect in this context is the investigation of the aircraft's aerodynamic properties and its flight dynamics. The demand for short runway length and thus low approach velocities imposes high requirements on the stabilizer and control surfaces design. The present report gives an overview on the ongoing investigations of the longitudinal and lateral aerodynamic behavior of the landing configuration. The influence of turboprop engines on the lateral motion is known [1,2], however documented investigations are limited in literature. Furthermore, it is assumed that the usage of circulation control (CC) has an additional impact, which shall be assessed, as well. Analogously, the effectiveness of the tail plane is also influenced by asymmetric engine [3, 4] and circulation control conditions. Previous investigations of the initial reference aircraft design proved the feasibility and potential of the single lift augmentation systems, when fully integrated into an aircraft [5, 6]. However, it also showed stronger

[†] Institut für Aerodynamik und Strömungstechnik, DLR Braunschweig

than expected restrictions on the maximum angle of attack and center of gravity position. The results were incorporated into a revised preliminary design, which was carried out in the course of the project. The last part of the present paper shows first results of the simulations of the improved design.

2. Numerical Method

The calculations are performed with the *DLR TAU* code [7], which is based on an unstructured finite volume approach for solving the Reynolds-averaged Navier-Stokes equations. For this investigation, the implicit LUSGS scheme is used for time stepping and a central scheme with scalar dissipation for the spatial discretization of the convective fluxes. The turbulence effects are modeled with the original Spalart-Allmaras formulation [8] with vortical and rotational flow correction based on the Spalart-Shur correction [9]. In order to model the turboprop engine, an actuator disk based on the 2D blade element theory is implemented. In this way, the local load of the propeller is calculated based on a given radial distribution of force coefficients along the blades and the local flow conditions [10]. The procedure already showed robust behavior and good results in various applications such as the simulation of a contra-rotating open rotor [11].

3. Geometry

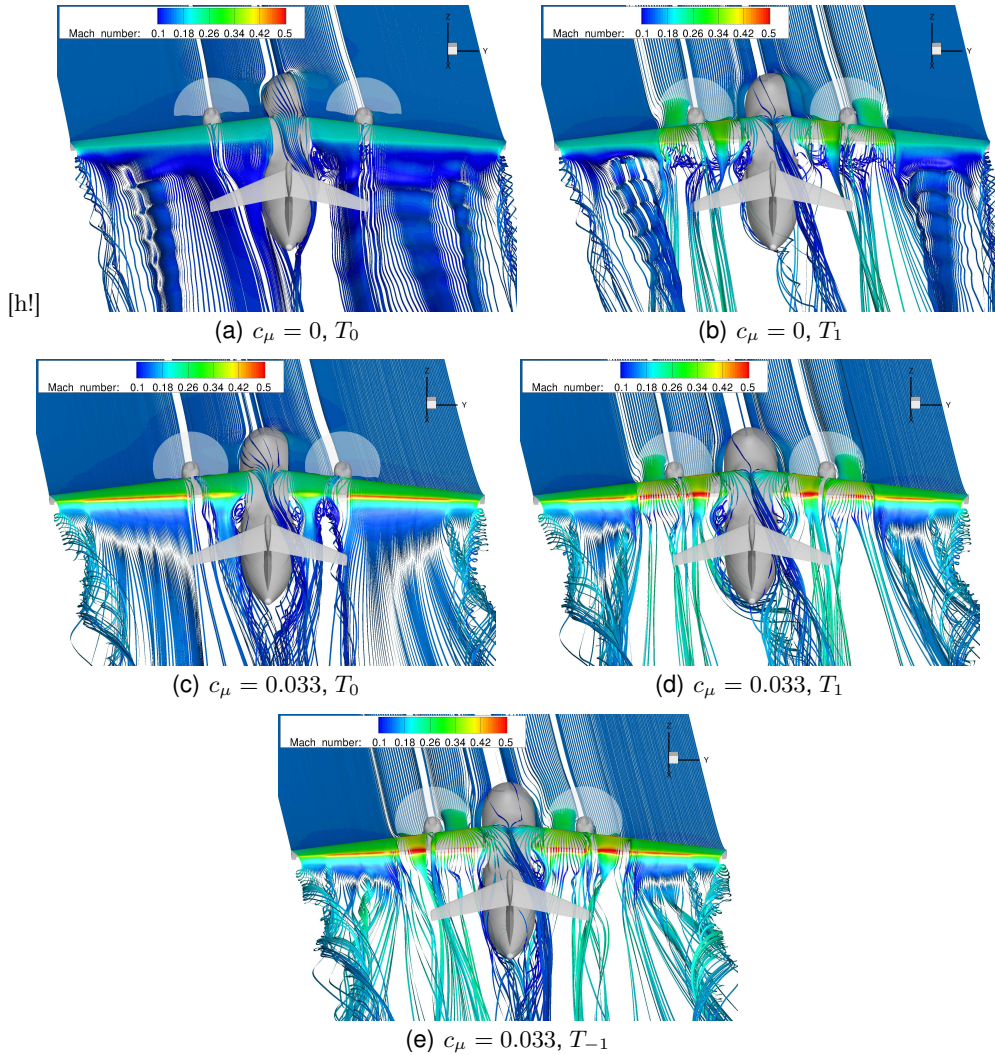
The first batch of simulations of the investigation were performed with the landing configuration of the initial PrADO [12] aircraft design *REF0-2011*. In this configuration, the internally blown flap is deflected by $\delta_{\text{Flap}} = 65^\circ$ and the ailerons are drooped by $\delta_{\text{Aileron}} = 45^\circ$. However, the aircraft does not utilize a leading edge device. For optimal efficiency of the circulation control, the plenum along the wing span is separated into six sections, which can be independently pressurized to adjust the blowing to the local flow conditions [5]. For the investigation of the lateral motion and the failure cases, the total pressure within the plenum was tuned to obtain fully attached flaps and ailerons at the smallest possible amount of blowing. At an angle of attack of $\alpha = 0.0^\circ$, the resulting global blowing coefficient is $c_\mu = 0.033$. In order to investigate the lateral motion and the failure cases, three different thrust settings are chosen, whereas the default rotational direction of the propeller is inboard up. Besides the zero thrust case (T_0), a moderate thrust setting (T_1) and the case of maximum thrust (T_2) are discussed. Furthermore, a case with the propeller rotating inboard down and same thrust setting as T_1 is also simulated (T_{-1}) in order to investigate the influence of the rotational direction.

As the RANS computations showed, the initial high-lift configuration had several drawbacks, which were addressed by a preliminary design update using PrADO. As a result, the size of the vertical as well as the horizontal tail planes is increased with the new design *REF2-2013*. Furthermore, the aircraft's main wing is tilted by $\Delta i_{\text{MW}} = -3.44^\circ$ and it utilizes a smart droop nose in order to allow higher angles of attack in high-lift configuration. The design update also resulted in an increased nacelle diameter.

4. Results

4.1. Lateral Motion

The lateral static behavior was investigated at an angle of attack of $\alpha = 0.0^\circ$. Besides the zero sideslip case, a moderate sideslip angle of $\beta = 5.0^\circ$ and a high sideslip angle


 FIGURE 1. Main wing wake evolution at sideslip ($\beta = 5.0^\circ$)

of $\beta = 11.4^\circ$ were simulated. The latter corresponds to the maximum required cross flow velocity of $v_Y = 20 \text{ knots}$ at reference flow conditions. Figure 1 shows the resulting main wing wake visualized by boundary layer streamlines for different blowing and engine conditions at $\beta = 5.0^\circ$. All conditions show a rotational flow behind the fuselage. However, the strength is influenced by circulation control and engine effects, i.e. different settings in c_μ and T . At zero thrust (T_0) and deactivated circulation control ($c_\mu = 0$) (Fig. 1(a)), the flow is completely separated from the trailing edge devices and the velocities above and behind the main wing are rather slow. The swirl behind the fuselage is also comparably small. Activating thrust (Fig. 1(b)) or circulation control (Fig. 1(c)) increases the circulation around the wing and thus the velocities above the wing and the swirl behind the fuselage rises. Activating both (Fig. 1(d)) amplifies the swirl. If the rotational direction of the propeller is changed to inboard down (Fig. 1(e)), the flow behind the fuselage is less distracted to the starboard side. The difference in the wake evolution

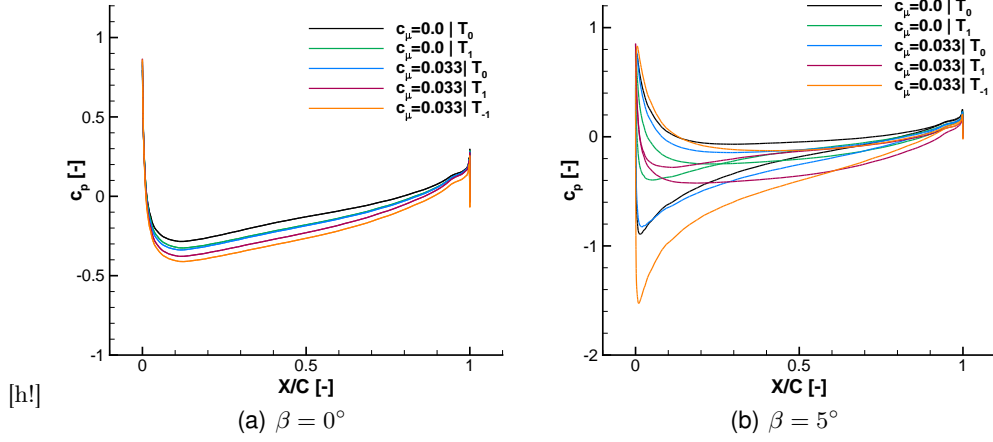


FIGURE 2. VTP pressure distribution at $\eta_{VTP} = 0.45$ for different circulation control and engine settings

also impacts the aerodynamics of the vertical tail plane. Figure 2 plots the pressure distributions for the different circulation control and engine settings at $\eta_{VTP} = 0.45$. At $\beta = 0^\circ$, the pressure distributions are symmetric and do not differ in shape. However, with activated circulation control and/or engines, the pressure along the VTP is reduced. At crossflow condition (Fig. 2(b)), the main wing wake influenced by circulation control and thrust leads to a reduced suction peak. However, the circulation control also causes a lower pressure in the rear part of the suction side. On the pressure side, the pressure level is reduced in both cases. While the change is rather small for activated circulation control without thrust ($c_\mu = 0.033, T_0$), it is already significant due to thrust only ($c_\mu = 0, T_1$). However, the change due to activated circulation control becomes large, when thrust is applied, as well ($c_\mu = 0.033, T_1$).

The trend seen in the pressure distributions can be also identified in the yawing moment coefficients (c_{Mz}) of the VTP with respect to sideslip (Fig. 3(a)). With no thrust, the vertical tail plane reacts with a stabilizing yawing moment to a sideslip angle of $\beta = 5^\circ$. The difference between activated and deactivated circulation control is negligible, here. When applying thrust, the yawing moment becomes slightly destabilizing, whereas the effect increases with activated circulation control. Changing the rotational direction of the propeller to inboard down leads to an increase of the stabilizing moment. When the sideslip angle is increased to $\beta = 11.4^\circ$, the impact of the circulation control and thrust seems to be reduced, resulting in positive yawing moments for all investigated cases. Besides the VTP, also the yawing moment of the fuselage is effected by circulation control and thrust (Fig. 3(b)). Again, the influence of circulation control is rather small, whereas the influence of thrust is significant. At $\beta = 5^\circ$, the fuselage also reacts destabilizing on sideslip in case of inboard up rotational direction of the propellers and stabilizing in the opposite case. However, at $\beta = 11.4^\circ$, also the thrust with inboard down rotational direction acts destabilizing. As a result, the aircraft is stable in case of deactivated engines and with activated engines and inboard down rotational direction of the propellers for small sideslip angles (Fig. 3(c)). In case of inboard up direction, the aircraft is laterally unstable for small sideslip angles.

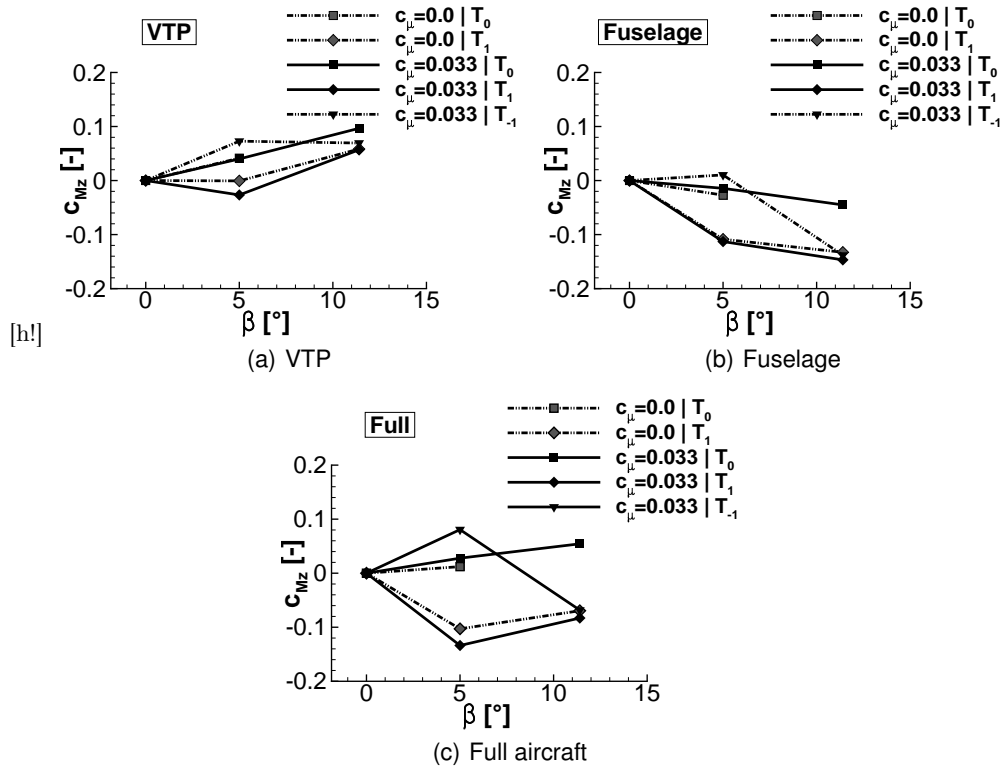


FIGURE 3. Yawing moment dependent on sideslip

4.2. System Failures

For twin-engine aircraft equipped with turboprop engines, the *one engine inoperative (OEI)* case becomes a dimensioning factor for VTP sizing. Due to large propellers, the engines have to be mounted further outboard and therefore create significant yawing moments. Furthermore, asymmetric thrust impacts the flow around the wing and the tail and thus alters their forces and moments. During take-off and landing, the dynamic pressure and therefore the forces of the control devices are low. Therefore, the *OEI* case has to be particularly considered in high-lift configuration. While the *OEI* case is critical for the yawing moment, an asymmetric failure of the circulation control (denoted as *CC failure*) is expected to be critical for the rolling moment. Since the engines are mounted symmetrically, there is no critical engine regarding *OEI*. For the simulation of the failure cases, the starboard mounted engine is deactivated. In case of the *CC failure*, the circulation control of the complete starboard wing is disabled.

The altered oncoming flow due to the engine deactivation as well as the deactivation of the circulation control influences the lift distribution of the main wing, as seen in Figure 4. With no failure case, the lift distribution is fully symmetric and peaks in the upwash region of the propeller. As expected, with an one-sided system failure, the lift distribution becomes asymmetric. While the distribution on the left wing is only slightly changed, the failure cases lead to a severe lift deterioration on the side of the system failures. In case of the *OEI*, the major lift reduction occurs at the inboard section of the wing in vicinity of the engine. For the failure of the circulation control system, the lift loss takes place

| Case | c_L [-] | c_D [-] | c_{My} [-] | $c_{My,WB}$ [-] | $c_{My,HTP}$ [-] |
|---------------------------------|-----------|-----------|--------------|-----------------|------------------|
| T_1 no failure | 3.66 | 0.7357 | 0.00 | 0.10 | 0.03 |
| T_1 <i>OEI</i> | 3.21 | 0.6065 | 0.08 | 0.22 | -0.09 |
| T_1 CC failure | 2.84 | 0.6239 | -0.04 | 0.16 | -0.08 |
| T_1 <i>OEI</i> CC failure | 2.39 | 0.5085 | -0.05 | 0.21 | -0.20 |

TABLE 1. Coefficients of the longitudinal motion in failure cases

over the entire half span. Even though the characteristics of the lift distribution do not change, its magnitude is reduced.

As a result, the global lift coefficient drops between 12% and 35% (Table 1) compared to the case with all engines operating and fully activated CC, depending on the failure case. Also, the pitching moment (c_{My}) is influenced. In all cases, the wing-body pitching moment changes in nose up direction. In contrast, the HTP pitching moment becomes negative due to the reduced downwash at the HTP. As a result, the aircraft tends to pitch up in case of *OEI* and to pitch down for the other cases.

Due to the asymmetric thrust and lift distribution, the flow behind the wing

evolves asymmetrically as well as it is seen in Figure 5. In contrast to case without failure (Fig. 5(a)), at *OEI*, the slipstream of the operating engine spreads out in spanwise direction and pushes the wake below the fuselage to the starboard side. Above the fuselage, the flow is deflected to the port side, as it was already observed by Mannée [3] and Schroyen et al. [2]. As they also concluded, the asymmetric lift distribution above the wing seems to be the origin of the side wash effect above the fuselage. The fact that a clear pressure gradient can be identified above the wing between the left and the right side and that the phenomena can be also seen in case of a circulation control failure (Fig. 5(c)) supports this assumption. Consequently, at *OEI* and circulation control failure, the rotational flow around the fuselage is also visible.

Figure 6 depicts the resulting pressure distributions at three different positions along the span of the VTP. As seen before, the pressure is slightly reduced when symmetric thrust is applied due to the increased velocities around the VTP. In case of an engine

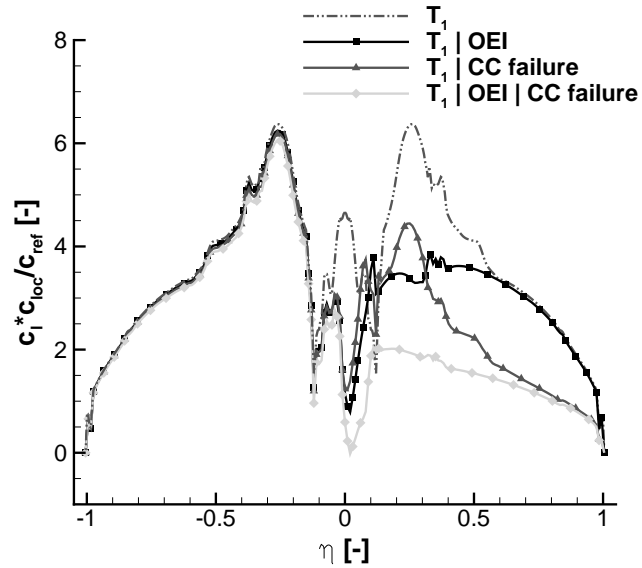


FIGURE 4. Lift distribution in asymmetric failure cases

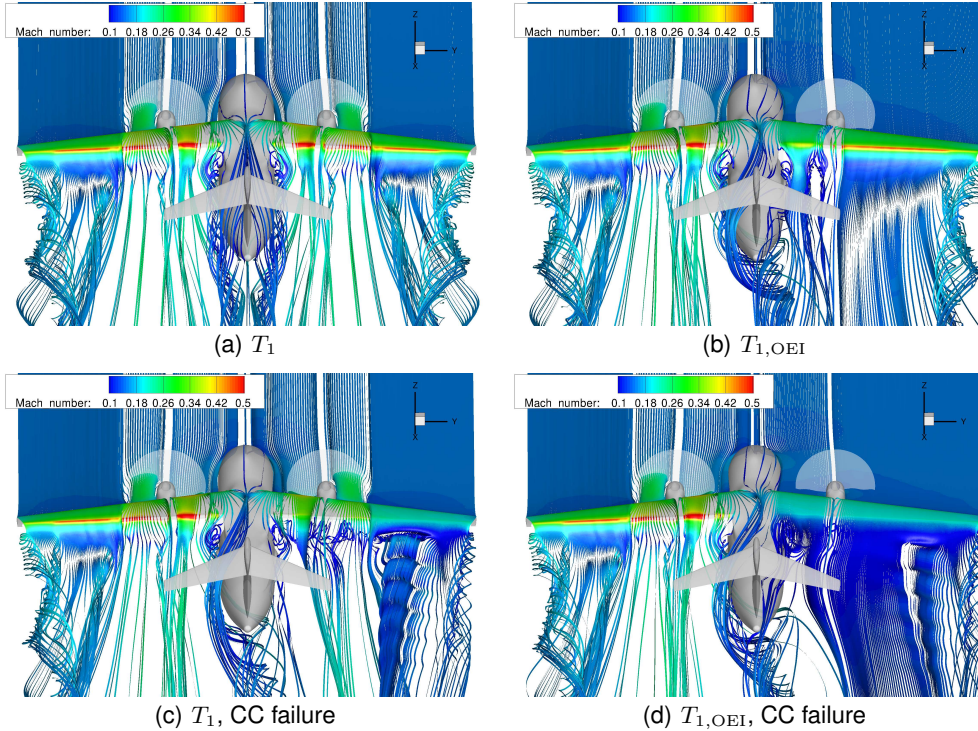


FIGURE 5. Main wing wake evolution

failure, the pressure distribution becomes asymmetric, showing lower pressures on the suction side with notable suction peaks at the nose and higher ones on the pressure side. While the change on the pressure distribution due to an engine failure or circulation control failure is already comparably large, it is the strongest if both systems fail. Also an increase in thrust (T_2) leads to a bigger impact. Even though, the suction peak is still smaller than in case of both failures at T_1 , the pressure is reduced more in the rear part of the suction side. Comparing the pressure sections with each other, it can be noticed that the suction peak decreases towards the VTP tip due to the decreasing sidewash, which is contrary to the typical suction peak distribution along a tapered lifting surface's span originated from the induced incidence angle. At $\eta_{VTP} = 0.7$, which is directly located below the HTP, the pressure distribution is impacted by the HTP's suction peak, leading to a pressure plateau between 20% and 40% of the local chord length.

Table 2 gives a detailed overview of the yawing moments for the different failure cases. As expected, the asymmetric thrust leads to a large negative yawing moment. In case of deactivated circulation control, the yawing moment can be almost completely attributed to the thrust. In contrast, if circulation control is activated, the yawing moment is significantly amplified, resulting in an increase of $\frac{\Delta C_{Mz, AF}}{C_{Mz, Prop}} = 126\%$ at T_1 and $\frac{\Delta C_{Mz, AF}}{C_{Mz, Prop}} = 88\%$ at T_2 . The additional moment can be mainly attributed to the fuselage and the VTP, which is in line with the pressure distributions in Fig 6. Also, the circulation control failure case shows a large yawing moment, even though the thrust is symmetric, here. The magnitude is comparable to the magnitude of the airframe's yawing moment at *OEI*. The fuselage's share of the yawing moment is even higher than the one in case of *OEI*. Comparing equal thrust settings, the VTP's yawing moment increases the most in case

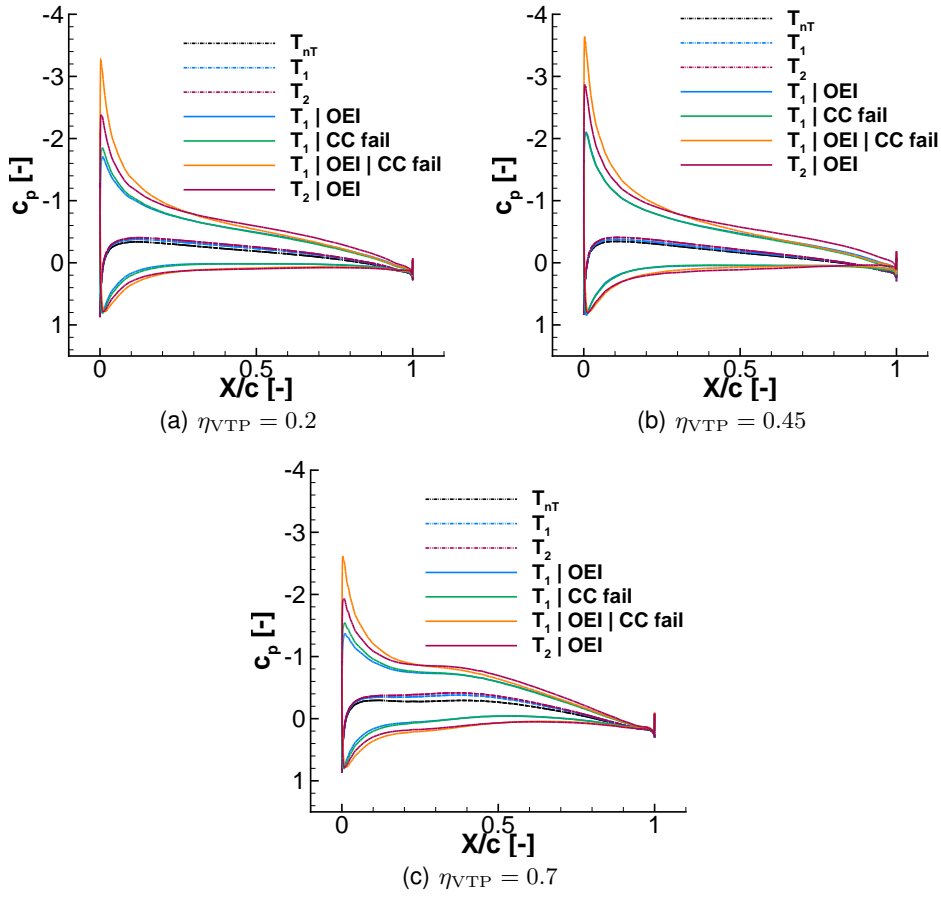


FIGURE 6. Pressure distribution along VTP in failure cases

| Case | Full | Propeller | c_{Mz} VTP | Fuselage | Wing |
|--|--------|-----------|-----------------|----------|-------|
| T_0 <i>OEI</i> | -0.148 | -0.127 | -0.033 | -0.028 | 0.036 |
| T_1 <i>OEI</i> | -0.286 | -0.127 | -0.103 | -0.109 | 0.046 |
| T_1 <i>CC failure</i> | -0.153 | 0.001 | -0.104 | -0.127 | 0.065 |
| T_1 <i>OEI</i> <i>CC failure</i> | -0.242 | -0.127 | -0.133 | -0.110 | 0.108 |
| T_2 <i>OEI</i> | -0.370 | -0.197 | -0.135 | -0.106 | 0.059 |

TABLE 2. Yawing moments in failure cases

of an engine and circulation control failure. However, the increase in thrust leads to the biggest raise in the VTP's yawing moment. Mostly due to the reduced induced drag of the starboard sided wing, the wing's contribution offsets the aircraft's yawing behavior to some extent. In summary, the *OEI* cases are, as expected, the most critical ones regarding the yawing moment. However, the magnitude of the aircraft's yawing moment

| Case | c_{Mx} | | | |
|---------------------------------|----------|-----------|-------|--------|
| | Full | Propeller | VTP | Wing |
| T_0 <i>OEI</i> | -0.095 | -0.020 | 0.007 | -0.082 |
| T_1 <i>OEI</i> | -0.086 | -0.023 | 0.021 | -0.090 |
| T_1 CC failure | -0.311 | 0.000 | 0.022 | -0.342 |
| T_1 <i>OEI</i> CC failure | -0.418 | -0.021 | 0.029 | -0.436 |
| T_2 <i>OEI</i> | -0.114 | -0.041 | 0.028 | -0.108 |

TABLE 3. Rolling moments in failure cases

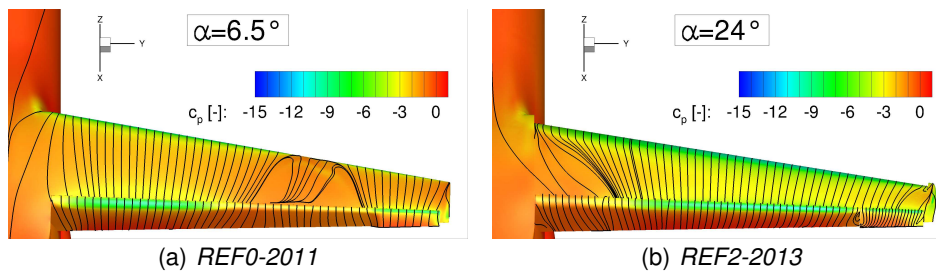


FIGURE 7. Comparison of post-stall pressure distribution on the main wing between old and new geometry

in these cases is unexpectedly high. It is also worth to note that a combination of both failures leads to a reduced yawing moment due to a higher wing contribution, which is acting in opposite direction of the other parts.

Table 3 shows the rolling moment coefficients (c_{Mx}) for the failure cases. As expected, the CC failure is more critical than the *OEI* case regarding the rolling moment. Here, the strongly reduced lift on the side of the deactivated CC leads to a dominating contribution of the rolling moment giving the aircraft the tendency of banking to the starboard side. If both systems fail, the rolling moment is further increased. Compared to the wing's share of the rolling moment, the stabilising contribution from the VTP is rather small. Furthermore, in case of an engine failure, the positive impact of the VTP's rolling moment is mostly equalized by the propeller torque of the running engine. Even though the rolling moment is a lot smaller in the *OEI* cases with fully activated CC, it is still significant.

4.3. Design Update

The integration of the droop nose and the reduction of the main wing's incidence angle aimed at increasing the maximum angle of attack. Figure 7 shows a comparison of the pressure distribution between the old geometry *REF0-2011* and the new geometry *REF2-2013* without engines at post-stall. While the *REF0-2011* stalled early ($\alpha_{\max, \text{REF0-2011}} = 6.0^\circ$ due to a leading edge separation on the outboard wing, the maximum angle of attack of *REF2-2013* could be delayed to $\alpha_{\max, \text{REF2-2013}} = 23^\circ$. Here, the maximum lift is limited due to increasing cross-flow and load reduction in the vicinity of the fuselage. Even though, the maximum angle of attack of the main wing without nacelle could be significantly increased, the consideration of the nacelle erodes

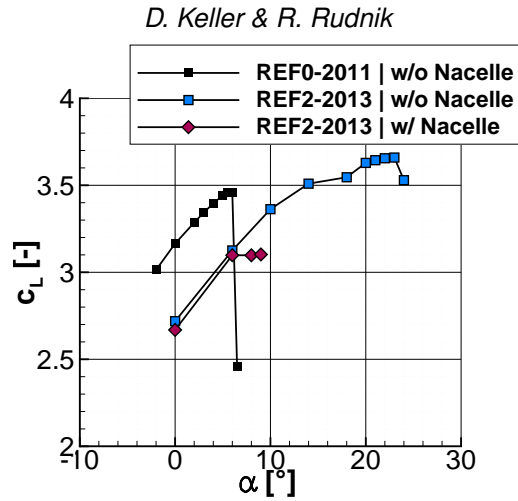


FIGURE 8. Comparison of lift coefficients over angle of attack between old and new geometry

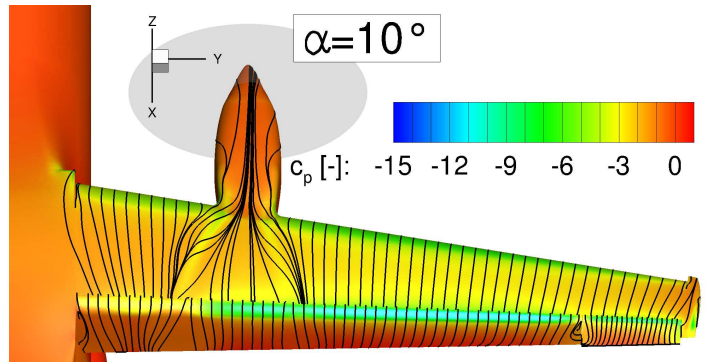


FIGURE 9. Post-stall pressure distribution of *REF2-2013* with nacelle and no thrust

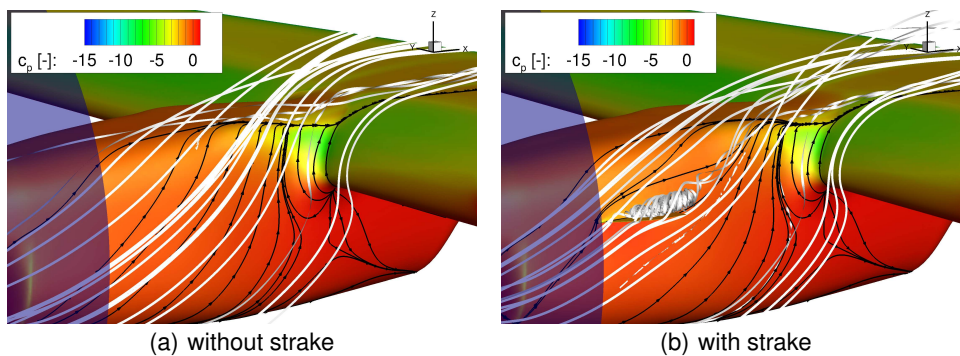
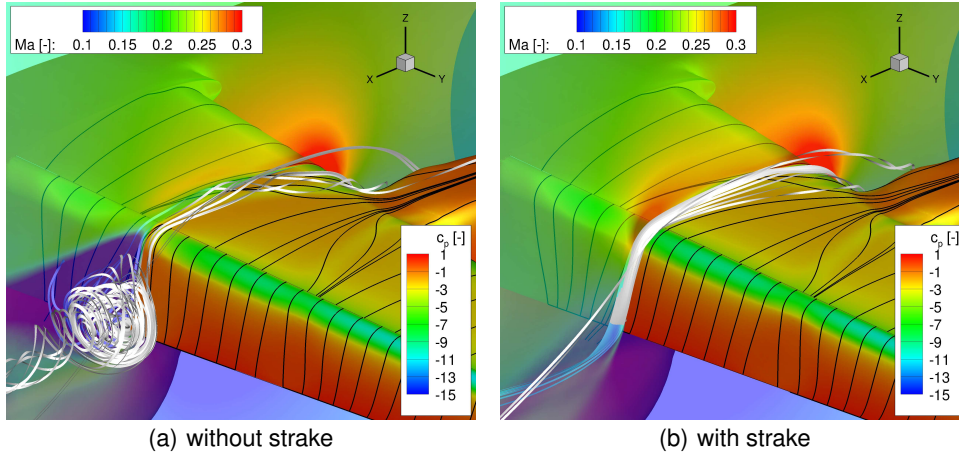


FIGURE 10. Flow conditions at the wing-nacelle junction at $c_{\mu} = 0.03$ and $\alpha = 10^\circ$

the improvement for the most part (Fig. 8). In this case, the stall is triggered by the inboard nacelle vortex (Fig. 9).

In order to improve the stall behavior with nacelle, a nacelle strake was added (Fig. 10), which is currently further investigated. First results already show an improvement of the flow conditions behind the nacelle (Fig. 11). If adequately positioned, the resulting

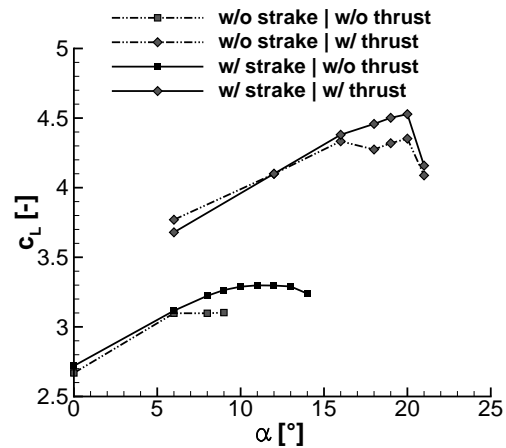

 FIGURE 11. Flow conditions behind nacelle at $c_{\mu} = 0.03$ and $\alpha = 10^{\circ}$

strake vortex suppresses the inboard nacelle vortex and leads to an attached flow on the flap even at higher angles of attack. As a result, the maximum angle of attack can be increased for several degrees in case of zero thrust (Fig. 12). Furthermore, the maximum lift coefficient is increased as well by $\Delta c_{L,w/othrust} = 0.19$. At a moderate thrust setting of $T = 49kN$ ($c_T = 0.24$), the maximum lift augmentation is comparable with $\Delta c_{L,w/thrust} = 0.18$. However, the maximum angle of attack remains unchanged.

5. Conclusion

The investigation of different engine and circulation control conditions in lateral motion demonstrates their strong impact on the directional stability. If thrust is applied, the existence of cross-flow leads to an altered flow around the fuselage and as a result to altered forces in the rear part of the aircraft. As a result, the aircraft is unstable in some cases. Circulation control amplifies the tendency, the aircraft shows without circulation control.

As expected, an engine failure leads to high yawing moments. However, the magnitude of the yawing moments is unexpectedly high, if circulation control is activated. In this case, the yawing moments of the aircraft can be more than twice as high as the actual ones due to the asymmetric thrust. Furthermore, *OEI* leads to considerable rolling moments due to the asymmetric lift augmentation originated from the slipstream. First simulations of the revised design (*REF2-2013*) show improvements in maximum lift and angle of attack, especially, when neglecting engine nacelles. With nacelles and without thrust, the enhancements are reduced to a different stall behavior. As a result, a nacelle strake was designed.


 FIGURE 12. Lift curve dependent on angle of attack of *REF2-2013*

It is shown, that the integration of the strake leads to an improvement in maximum lift and maximum angle of attack at zero thrust and to a maximum lift gain when thrust is applied.

References

- [1]R. S. van Rooyen and M. E. Eshelby. Assessment of propeller influence on lateral-directional stability of multiengine aircraft. volume 18 of *Journal of Aircraft*, pages 364–371. 1981.
- [2]M.J.T. Schroyen, L.L.M. Veldhuis, and R. Slingerland. Propeller slipstream investigation using the fokker f27 wind tunnel model with flaps deflected. Paper, Anchorage, Alaska, September 2008. Proceedings of the ICAS 2008 Congress.
- [3]J. Mannée. Windtunnel Investigation of the Influence of the Aircraft Configuration on the Yawing and Rolling Moments of a Twin-Engined Propeller Driven Aircraft with one Engine Inoperative. Technical report, Amsterdam, 1962.
- [4]M.J.T. Schroyen, L.L.M. Veldhuis, and R. Slingerland. Propeller Empennage Interaction Effects on Vertical Tail Design of Multiengine Aircraft. volume 47 of *Journal of Aircraft*, pages 1133–1140. 2010.
- [5]D. Keller. Numerical Approach Aspects for the Investigation of the Longitudinal Static Stability of a Transport Aircraft with Circulation Control. volume 124 of *Notes on Numerical Fluid Mechanics and Multidisciplinary Design*, pages 13–22. Springer, 2014.
- [6]D. Keller and R. Rudnik. Aerodynamic Aspects of the Longitudinal Motion of a High-Lift Aircraft Configuration with Circulation Control. In Rolf Radespiel and Richard Semaan, editors, *TU Braunschweig - Campus Forschungsflughafen, Berichte aus der Luft- und Raumfahrttechnik*, number 2013-3. Shaker Verlag, 2013.
- [7]T. Gerhold. Overview of the Hybrid RANS Code TAU. In N. Kroll and J. Fassbender, editors, *MEGAFLOW – Numerical Flow Simulation for Aircraft Design*, volume 89 of *Notes on Numerical Fluid Mechanics and Multidisciplinary Design*, pages 81–92. Springer, 2005.
- [8]P.R. Spalart and S.R. Allmaras. A One–Equation Turbulence Model for Aerodynamic–Flows. AIAA Paper 92–0439, 1992.
- [9]P.R. Spalart and M. Shur. On the sensitization of turbulence models to rotation and curvature. volume 1 of *Aerospace Science and Technology*, pages 297–302. 1997.
- [10]A. Raichle. A new Actuator Disk Model for the TAU Code and application to a sailplane with a folding engine. In *Notes on Numerical Fluid Mechanics and Multidisciplinary Design: New Results in Numerical and Experimental Fluid Mechanics VI*, Darmstadt, Germany, 2006. Contributions to the 15th DGLR-STAB Symposium.
- [11]C. O. Marquez Gutierrez. Validation of Actuator Disk Simulations of CROR Propulsion Systems at Low-Speed Flight Conditions. New Orleans, USA, 2012. American Institute of Aeronautics and Astronautics.
- [12]W. Heinze, C. M. Österheld, and P. Horst. Multidisziplinäres Flugzeugentwurfsverfahren PrADO - Programmwurf und Anwendung im Rahmen von Flugzeug-Konzeptstudien. In Bonn Deutsche Gesellschaft für Luft-und Raumfahrt (DGLR), editor, *DGLR-Jahrbuch 2001*, volume 3, pages 1701–1712. Bonn, 2001.